*Supporting Information*

# Infrared Detection with Temperature Sweep for Stability Determination of Ru-ON Metastable States

Vasily Vorobyev*[,†,‡,§], Nina I. Alferova[‡], and Vyacheslav A. Emelyanov[†,‡]

[†]Department of Natural Sciences, Novosibirsk State University, Novosibirsk 630090, Russia

[‡]Nikolaev Institute of Inorganic Chemistry, Siberian Branch of the Russian Academy of Science, Novosibirsk 630090, Russia

[§]Department of Chemistry and the Center for Photochemical Sciences, Bowling Green State University, Bowling Green, Ohio 43402, United States

# Table of content



# Table S1

The studied complexes with **GS** and **MS1** spectroscopic properties and stability (ordered by **MS1** wavenumber). The accuracy of $E_a$, $k_o$, and $T_d$ are on 5 kJ mol$^{-1}$, 1, and 3 K levels.

| N | Complex and synthetic reference | ν(NO) **GS**, cm$^{-1}$ | ν(NO) **MS1**, cm$^{-1}$ | $E_a$, kJ mol$^{-1}$ | log $k_o$ | $T_d$, K | **MS1** Stability |
|---|---|---|---|---|---|---|---|
| **1** | *trans*-$[RuNO(NH_3)_4OH]Cl_2$[1] | 1849 | 1716 | 87.8 | 14.8 | 258 | [2] |
| **2** | *trans*-$[RuNO(NH_3)_2(NO_2)_2OH]$[3] | 1859<br>1879 | 1736<br>1758 | 55.4<br>57.5 | 11.0<br>13.0 | 206<br>188 | a) |
| **3** | *cis*-$[\{RuNO(NH_3)_2Cl_2\}_2(H_3O_2)]Cl$[4] | 1872 | 1740 | 69.0 | 12.0 | 240 | b) |
| **4** | *cis*-$Cs[RuNO(NH_3)Cl_4]\cdot H_2O$[c] | 1881 | 1743 | 53.6 | 12.4 | 182 | b) |
| **5** | *mer*-$[RuNO(NH_3)_3Cl_2]Cl\cdot H_2O$[5] | 1888 | 1755 | 59.9 | 10.9 | 225 | b) |
| **6** | *mer*(*trans*)-$[RuNO(NH_3)_2Cl_3]$[6] | 1884 | 1756 | 46.5 | 9.3 | 197 | b) |
| **7** | *fac*-$[RuNO(NH_3)_2Cl_3]$[7] | 1884 | 1758 | 57.7 | 11.8 | 203 | b) |
| **8** | *cis*-$[RuNO(NH_3)_2(NO_2)_2OH]$[8] | 1882<br>1907 | 1758<br>1780 | 54.9<br>54.2 | 10.4<br>10.2 | 214<br>214 | a) |
| **9** | *tr*-$[RuNO(NH_3)_2Cl_2(H_2O)]Cl\cdot 2H_2O$6 | 1903 | 1770 | 94.1 | 18.1 | 233 | b) |
| **10** | *fac*-$K_2[RuNO(NO_2)_2Cl_3]$[9] | 1900 | 1774 | 60.5 | 13.5 | 192 | d) |
| **11** | *mer*(*cis*)-$[RuNO(NH_3)_2Cl_3]$[c] | 1904 | 1778 | 47.2 | 10.8 | 181 | b) |
| **12** | *mer*-$[RuNO(NH_3)_3Cl(H_2O)]Cl_2$[10] | 1923 | 1780 | 62.6 | 10.8 | 237 | b) |
| **13** | *tr*-$[RuNO(NH_3)_2(NO_3)_2(H_2O)]NO_3\cdot H_2O$3 | 1923 | 1790 | 74.3 | 12.3 | 254 | b) |
| **14** | $[RuNO(NH_3)_5]Cl_3\cdot H_2O$[11] | 1911 | 1799 | 70.4 | 12.0 | 245 | [12] |
| **15** | *mer*-$[RuNO(NH_3)_3(NO_2)(H_2O)](NO_3)_2$[13] | 1930 | 1810 | 47.4 | 8.2 | 220 | b) |
| **16** | *fac*-$[RuNO(NH_3)_2(NO_3)_3]$[14] | 1938 | 1813 | 64.8 | 12.2 | 223 | b) |
| **17** | *fac*-$[RuNO(NH_3)_3(NO_2)_2]NO_3$[15] | 1926 | 1813 | 71.6 | 12.7 | 239 | b) |
| **18** | *fac*-$[RuNO(NH_3)_3(NO_3)_2]NO_3\cdot H_2O$[c] | 1936 | 1818 | 37.3 | 6.5 | 199 | b) |

[a] $E_a$ and $k_o$ found from isothermal IR experiments in this work [b] $E_a$ and $k_o$ found by proposed IR detection with temperature swipe [c] structure and synthesis mentioned in the supporting information [d] $E_a$ and $k_o$ found by DSC in this work

## DSC of *fac*-$K_2[RuNO(NO_2)_2Cl_3]$ (10)

The kinetic and thermal effects of the **MS1**-to-**GS** transition were studied using a NETZSCH DSC 204 F1 Phoenix differential scanning calorimeter. The heat-flow between open aluminum crucibles with powdered samples (1-3 mg) was recorded (Figure S1). For the generation of the *O*-coordinated nitrosyl species in the solid phase, the samples was irradiated in a liquid nitrogen bath with 443 nm light, same as in the IR experiments. Then, the sample was transferred to the instrument and heated up at a constant heat rate of 6, 9, or 12 K/min; the Ar gas flow was 25 mL/min. To increase the accuracy, measurements were performed without supplying liquid or gaseous nitrogen into the cell during the experiment. To calibrate the sample holder sensor and temperature scale, standard samples were melted ($C_6H_{12}$, Hg, In) or the crystal-to-crystal transition was measured ($KNO_3$).

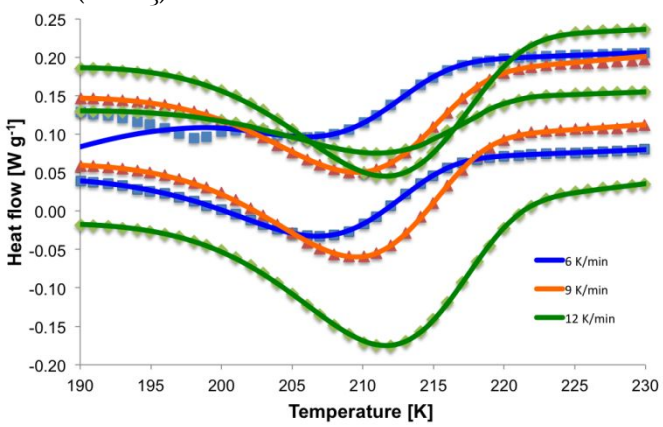


Figure S1. The experimental DSC data for the **MS1** decay in *fac*-$K_2[RuNO(NO_2)_2Cl_3]$ (**10**) are in dots. Solid lines are the first order kinetic fit with $E_a$ = 60.5±1.9 kJ mol$^{-1}$ and log $k_o$ = 13.46±0.49.

Processing of the experimental data was performed in Microsoft Excel for Mac 2011 based on the following equations and assumptions. The rate of the **MS1**-to-**GS** transition obeys the first-order reaction with the rate constant following the Arrhenius law $k = k_0 \cdot e^{-\frac{E_a}{RT}}$ (Eq. S1), where $k_o$ and $E_a$ are pre-exponential factor and activation energy. The actual rotation from 0° to 180° passes the 90° Ru-N-O angle, where the **MS2** local minima is positioned. In the case of $[RuNO(CN)_5]^{2-}$ and $[OsNO(CN)_5]^{2-}$, the thermal decay of the **MS1** ends up in the **MS2** rather than in the ground state since the **MS2** is more stable ($T_d$ are 240 and 220 K) than the corresponding **MS1** (230 and 190 K). [16] These two complexes are exceptional exemplars of the thermal **MS1**-to-**MS2** transformation; however, the most nitrosyl ruthenium complexes passes **MS2** on the way to **GS** without hesitation because the decay of **MS2** is generally faster than it's thermal generation from **MS1**. Thus, the implemented model took in account the **MS1** as a reactant and **GS** as a product. In the case of **MS2** being more stable than **MS1**, an additional thermal effect is expected to be observed at higher temperatures with comparable integral intensity. In terms of the proposed method based on IR detection with temperature sweep, passing by the **MS2** intermediate state would not have an impact on the monitored nitrosyl valence vibration

(**MS2** absorbs about 300 cm$^{-1}$ lower than **GS**). In terms of the observed kinetics, the **MS2** being a product would not have impact on the depletion rate of **MS1** because the possible **MS2**-to-**MS1** transformation is photodriven.[17]

Once the sample being heated up to a certain temperature, the **MS1** begin to rotate back to ground state with stored heat being released **MS1** → **GS** + Q with a rate law expressed as $-\frac{d\mathbf{MS1}}{dt} = k(T) \cdot [\mathbf{MS1}]$, where $k(T)$ is dependent on the temperature. Multiplying by enthalpy of the **MS1**-to-**GS** transition, $\Delta H$, gives the heat flow associated with the **MS1** decay $\dot{H} = \frac{dQ}{dt} = k(T) \cdot \Delta H \cdot [\mathbf{MS1}]$ (Eq. S2). Time, recorded temperature and heat flow are the instrument output which were fitted with a set of three parameters ($k_0$, $E_a$, and $\Delta H$), variable baseline (simple linear f($T$) function) and Eq. S1 and S2. The starting **MS1** concentration was taken as unity which degrades on each time point according to the calculated $k(T)$ at this point as $[\mathbf{MS1}](t) = [\mathbf{MS1}](t - \Delta t) \cdot e^{-k(T) \cdot \Delta t}$.

It was hard to solve the system of Eq. S1 and S2 numerically, but one iterative formula can be derived. The temperature at which the maximum heat flow occurs is equal to $T_{max} = \frac{E_a}{R \cdot \ln \frac{R \cdot k_0 \cdot T_{max}^2}{heat\ rate \cdot E_a}}$. This formula is useful for connecting of the old data of the **MS1** decay where the peak maximum is reported at the 5 K/min heat rate. To the accuracy of 2 K, the peak maximum is shifted to the higher temperature by 15 K at this specific heat rate compare to $T_d$. Also, the maximum heat flow shifts to the higher temperature as the heating goes up as observed on the Figure S1.

## Isothermal IR of Ru-ON in *cis*- and *trans*-[RuNO(NH$_3$)$_2$(NO$_2$)$_2$OH]

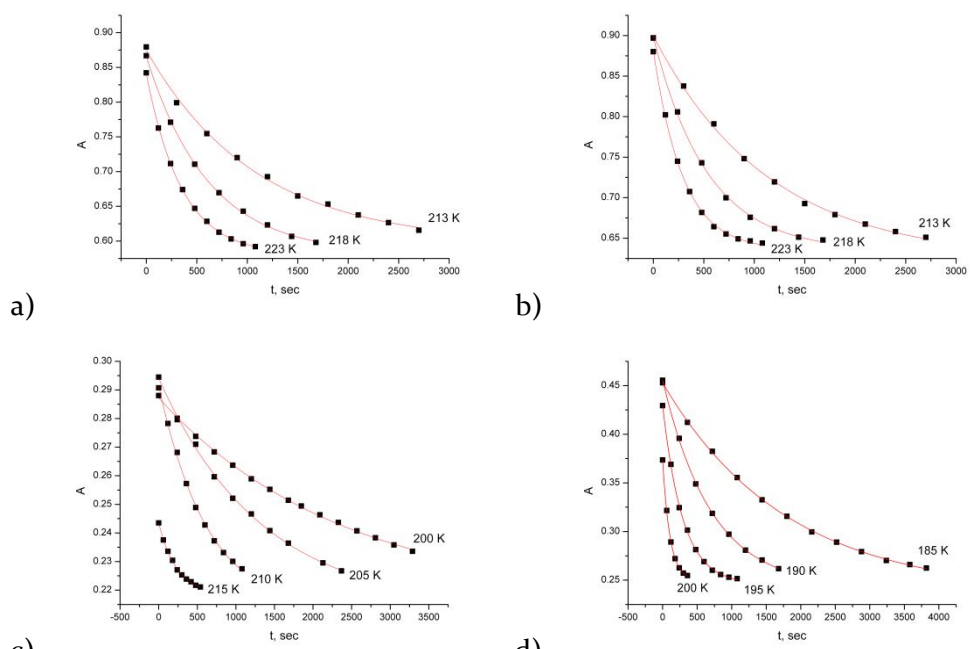


Figure S2. Experimental (dots) and fitted absorption loss (unimolecular, lines) of the Ru-ON states in *cis*-[RuNO(NH$_3$)$_2$(NO$_2$)$_2$OH] (**8**). (ν(NO) positioned at 1760 cm$^{-1}$ in a), 1781 cm$^{-1}$ in b)). and *trans*-[RuNO(NH$_3$)$_2$(NO$_2$)$_2$OH] (**2**) (ν(NO) at 1736 cm$^{-1}$ in c), 1756 cm$^{-1}$ in d)).

## Comments to the heating of KBr disk

Addition of the nitrosyl complexes with known thermal stability reveals the heating profile based on the known **MS** decay. Since the tested complex is mixed in the same disk, the $T(t)$ is the same for all mixed-in complexes and the thermal stability can be evaluated from the observed absorbance loss of the corresponding ν(NO).

The pressed KBr disc has polycrystalline nature and contains absorbed water up to 0.033%.[18] The disk shrinks while cooling in the liquid nitrogen. Upon transferring to the warm sample holder, the crystals thermally expand and cause disk opacification. Microscopic cracks work as a fingerprint on the optic cuvette. In terms of the IR spectroscopy, smaller amounts of light are transmitted at every wavelength. Once the temperature hits -12.6 °C, the ice melts to give a saturated KBr solution on the crystal surfaces. Fractures made by thermal shrinking-expansion are filled by this solution, making the disk more transparent, and in turn, the spectral baseline goes back to the normal values. The disk pressed with higher pressure from perfectly dry, well-grounded KBr would not have that baseline fluctuation. But the fluctuation provides one more temperature point needed for the heat rate evaluation.

The Gram-Schmidt reconstruction of the IR data extracts the thermal baseline variation into a separate data set. The spectral data is no longer dependent on the background and the extracted background absorption has a pronounced minimum. This point has reproducible temperature of 258.1(1.5) K among ten measurements. The temperature value was derived from the studies in which the temperature function can be derived based only on the known **MS1** properties. For example, the known thermal properties of the metastable states in the complexes **1** and **14** allows to derive the temperature profile in the mixture of the complexes **1**, **14**, **16** or in the mixture of **1**, **3**, **14** (Fig. S5B, S5C). Once the average of ten ice-melting points was calculated, the ice-melting point as 258.1 K was used as a reference point and the data was re-fitted using new reference ice-melting point. Difference of 2.5 K from the minimum point on the KBr-water phase diagram can be attributed to the local defects.

Going back to the $T(t)$ function, the only variable for adjustment is the starting time. The starting temperature (78 K), the sample holder temperature (293 K), and the ice-melting (258.1 K) time point are known. The starting time was adjusted based on a mixed-in compound with known **MS1** thermal properties. Based on the known *T(t)* function, the first-order kinetic model requires two variables, $E_a$ and $k_o$, to define the decay of a chosen **MS1** fraction from unity to zero. The $E_a$ and $k_o$ were adjusted for the model to match the normalized experimental **MS1** absorption curve.

## Comments to the data processing

The input data contained Gram-Schmidt intensities, $I_{G\text{-}S}(t)$, and integrated absorption of the **MS1** bands under study, $A(t)$. Integration was done in the program set provided by the manufacturer of the IR instrument (VERTEX 80v). Processing of the experimental data was performed in Microsoft Excel for Mac 2011 based on the following equations and assumptions. The minimum point of the $I_{G\text{-}S}(t)$ curve was set as 258.1 K for $t_{\text{ice melting}}$. For the initial guess, the starting time, $t_{\text{start}}$, was set for the moment of random jumps on $I_{G\text{-}S}(t)$ and $A(t)$ curves. At this moment, the sample was installed in the holder and the scanning light was blocked during installation period. To find the heating rate constant of $T(t) = T_{end} + (T_{start} - T_{end})\cdot e^{-k\cdot t}$ equation (Eq. S3), the $k$ equal to $\ln((T_{start} - T_{end})/(258.1 - T_{end}))/(t_{\text{ice melting}} - t_{\text{start}})$ (Eq. S4) was derived. Later on, the $t_{\text{start}}$ will be adjusted for better match through changes in Eq. S4 leading to changes in $T(t)$ function.

The amount of a chosen **MS1**, $\omega(t)$, was set to unity at $t$=0. At a moment $t$, the rate constant of the **MS1**-to-**GS** conversion is equal to $k(t)=k_0\cdot\exp[-E_a/RT(t-t_{start})]$ (Eq. S5), where $T(t)$ comes from Eq. S3; $E_a$ and $k_0$ correspond to the chosen **MS1**. If these values are not known, they will be subject of adjustment. At the next time step, $t$+d$t$, some **MS1** rotate back to **GS** and $\omega(t+dt)=\omega(t)\cdot\exp[dt\cdot k(t+dt)]$ (Eq. 4), where $k(t+dt)$ is Eq. S5. From a known amount of the chosen **MS1**, the absorbance curve was found as $A_{fit}(t) = \omega(t)\cdot(A_{start}-A_{end})+A_{end}$ (Eq. S7), where $A_{start}$ and $A_{end}$ are adjustable initial and final absorbance.

The residual sum of squares of modeled $A_{fit}(t)$ and experimental $A(t)$ was minimized by adjustment of parameters. For the compounds acting as internal temperature probe in the studied KBr disk, the parameters to adjust were $A_{start}$, $A_{end}$, and $t_{start}$. Availability of long time periods before and after **MS1** decay gives precise estimation of the first two parameters. For the several internal standards in the disk, the residual sum of squares was minimized for two and more modeled $A_{fit}(t)$ and experimental $A(t)$ by adjustment of individual $A_{start}$ and $A_{end}$ for each compound and a single $t_{start}$ for the whole KBr disk. The $A_{start}$ and $A_{end}$ were used later to plot normalized experimental absorbance $A_{normalized}(t) = (A(t)-A_{end})/(A_{start}-A_{end})$ (Eq. S8).

For the complexes with unknown **MS1** thermal stability parameters, the residual sum of squares of modeled $A_{fit}(t)$ and experimental $A(t)$ was minimized by adjustment of different set of parameters. The $A_{start}$, $A_{end}$, $E_a$, and $k_0$ were adjusted. The $t_{start}$ was used at it was found from the known complexes adjustment. The normalized absorption was calculated from Eq. S8.

## *cis*-Cs[RuNO($NH_3$)$Cl_4$]·$H_2O$ (4)

The complex *cis*-Cs[RuNO($NH_3$)$Cl_4$]·$H_2O$ (**4**) obtained as a minor product in the reaction of *trans*-[RuNO($NH_3$)$_4$OH]$Cl_2$ with 16 M $HNO_3$ (Kabin E. V., et al. *Russ. J. Inorg. Chem.* **2012**, 57(8), 1146). Excess of nitric acid was removed by reaction with excess of hydrochloric acid; the $[RuNOCl_5]^{2-}$ anion was precipitated as insoluble $Cs_2[RuNOCl_5]$ after addition of CsCl. The desired monoammine complex was the only soluble ruthenium complex after the performed manipulations. Yield was 10%. The compound was recrystallized from water to obtain single crystals suitable for X-ray studies (Fig. S3).

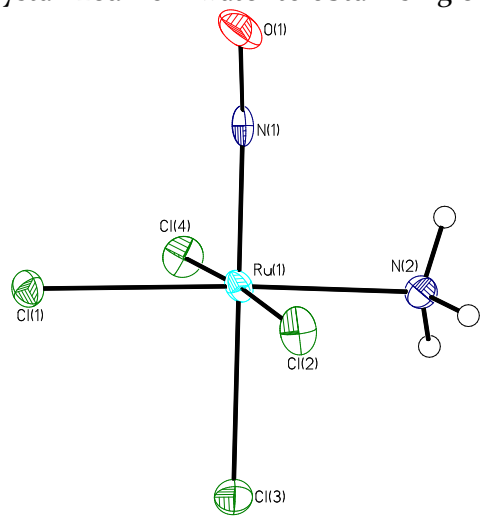


Fig. S3. The structure of the tetrachloroamminenitrosylruthenate in *cis*-Cs[RuNO($NH_3$)$Cl_4$]·$H_2O$ (**4**).

## *mer*(*cis*)-[RuNO($NH_3$)$_2$$Cl_3$] (**11**)

The complex *mer*(*cis*)-[RuNO($NH_3$)$_2$$Cl_3$] with *trans*-ON-Ru-$NH_3$ coordinate was synthesized in the modified procedure of *fac*-[RuNO($NH_3$)$_3$$Cl_2$]Cl synthesis (Vorobyev V., et al. *Eur. J. Inorg. Chem.* **2017**, (5), 971). The mixture of concentrated ammonia with sodium hexanitroruthenate was neutralized by excess of hydrochloric acid after the ruthenium complexes dissolved. The mixture was kept in the ice bath to avoid overheating. Insoluble trichloro complex precipitated after gentle heating of the acidic solution. Suitable for X-ray crystals were obtained by recrystallization in 6 M HCl (Fig. S4).

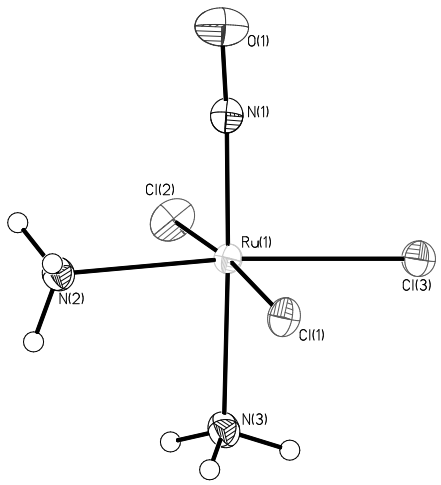


Figure S4. The structure of *mer*(*cis*)-[RuNO($NH_3$)$_2$$Cl_3$] (**11**).

## *fac*-[RuNO($NH_3$)$_3$($NO_3$)$_2$]$NO_3$·$H_2O$ (**18**)

The facial triammine complex was synthesized by using of 3 M nitric acid instead of hydrochloric acid in the *fac*-[RuNO($NH_3$)$_3$$Cl_2$]Cl synthesis (Vorobyev V., et al. *Eur. J. Inorg. Chem.* **2017**, (5), 971). Yield was 84%. Unfortunately, the complex crystallizes in highly symmetric F-43m space group with randomly distorted ligands around the central ruthenium atom. The composition of the complex was validated by elemental analysis. Found: N – 25.8(4), H – 2.9(5), calculated: N – 25.4, H – 2.9%.

## Normalized MS1 absorptions in the tested mixtures

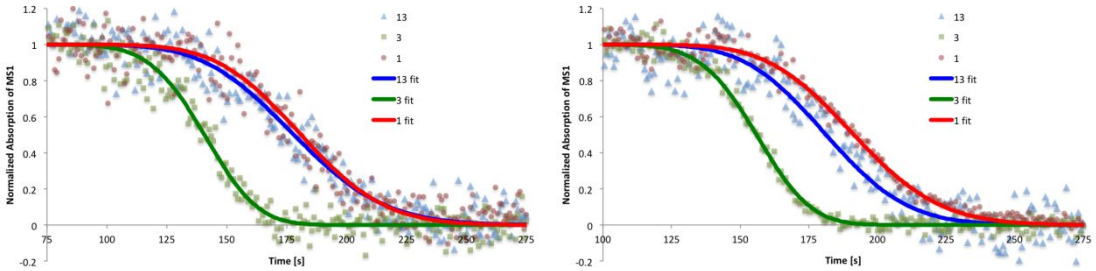


Figure S5A. Two independent studies of the mixture of *trans*-[RuNO($NH_3$)$_4$OH]$Cl_2$ (**1**), *cis*-[{RuNO($NH_3$)$_2$$Cl_2$}$_2$($H_3O_2$)]Cl (**3**), and *trans*-[RuNO($NH_3$)$_2$($NO_3$)$_2$($H_2O$)]$NO_3$·$H_2O$ (**13**). The complex **1** was an internal standard.

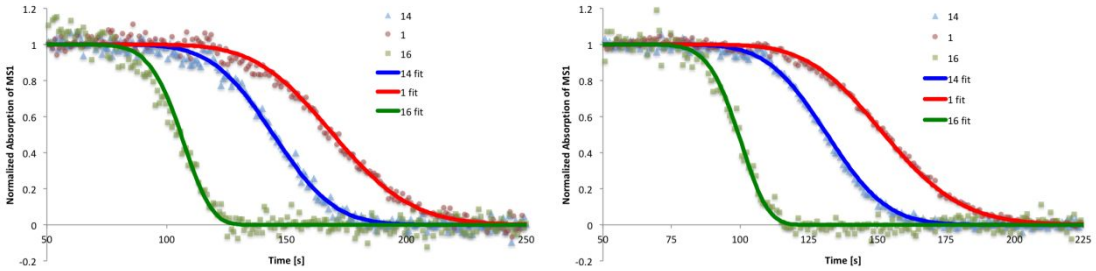


Figure S5B. Two independent studies of the mixture of *trans*-$[RuNO(NH_3)_4OH]Cl_2$ (**1**), $[RuNO(NH_3)_5]Cl_3{\cdot}H_2O$ (**14**), and *fac*-$[RuNO(NH_3)_2(NO_3)_3]$ (**16**). The complexes **1** and **14** were internal standards.

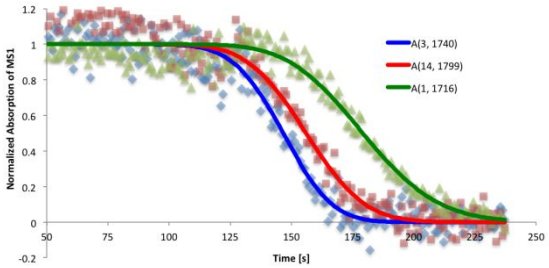


Figure S5C. Mixture of *trans*-$[RuNO(NH_3)_4OH]Cl_2$ (**1**), *cis*-$[\{RuNO(NH_3)_2Cl_2\}_2(H_3O_2)]Cl$ (**3**), $[RuNO(NH_3)_5]Cl_3{\cdot}H_2O$ (**14**). The complexes **1** and **14** were internal standards.

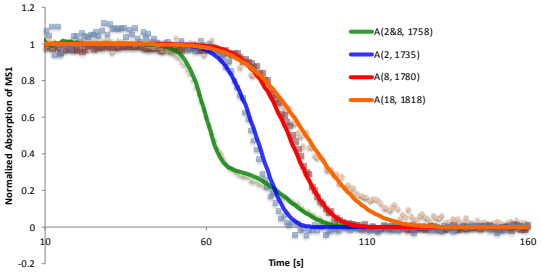


Figure S5D. Mixture of *trans*-$[RuNO(NH_3)_2(NO_2)_2OH]$ (**2**), *cis*-$[RuNO(NH_3)_2(NO_2)_2OH]$ (**8**), and *fac*-$[RuNO(NH_3)_3(NO_3)_2]NO_3{\cdot}H_2O$ (**18**). The complexes **2** and **8** were internal standards.

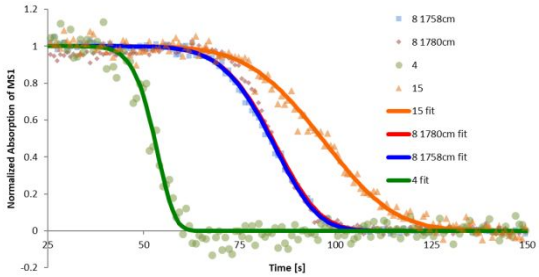


Figure S5E. Mixture of *cis*-$Cs[RuNO(NH_3)Cl_4]{\cdot}H_2O$ (**4**), *cis*-$[RuNO(NH_3)_2(NO_2)_2OH]$ (**8**), and *mer*-$[RuNO(NH_3)_3(NO_2)(H_2O)](NO_3)_2$ (**15**). The complex **8** was an internal standard.

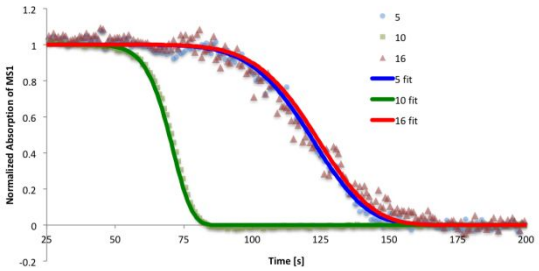


Figure S5F. Mixture of *mer*-$[RuNO(NH_3)_3Cl_2]Cl{\cdot}H_2O$ (**5**), *fac*-$K_2[RuNO(NO_2)_2Cl_3]$ (**10**), and *fac*-$[RuNO(NH_3)_2(NO_3)_3]$ (**16**). The complex **10** was an internal standard.

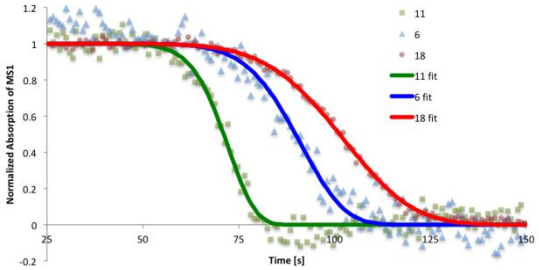


Figure S5G. Mixture of *mer*(*trans*)-$[RuNO(NH_3)_2Cl_3]$ (**6**), *mer*(*cis*)-$[RuNO(NH_3)_2Cl_3]$ (**11**), and *fac*-$[RuNO(NH_3)_3(NO_3)_2]NO_3{\cdot}H_2O$ (**18**). The complex **18** was an internal standard since it was studied in other mixture (Fig. S5D).

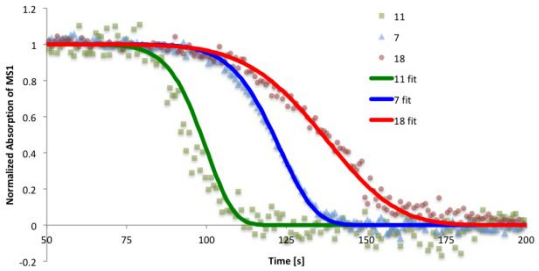


Figure S5H. Mixture of *fac*-$[RuNO(NH_3)_2Cl_3]$ (**7**), *mer*(*cis*)-$[RuNO(NH_3)_2Cl_3]$ (**11**), and *fac*-$[RuNO(NH_3)_3(NO_3)_2]NO_3{\cdot}H_2O$ (**18**). The complex **18** was an internal standard since it was studied in other mixture (Fig. S5D).

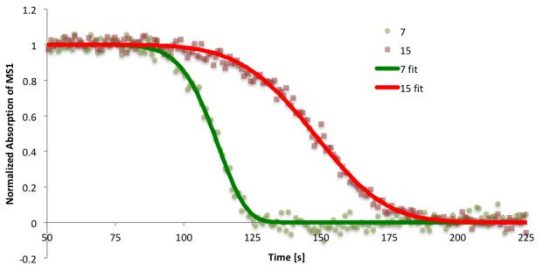


Figure S5I. Mixture of *fac*-$[RuNO(NH_3)_2Cl_3]$ (**7**) and *mer*-$[RuNO(NH_3)_3(NO_2)(H_2O)](NO_3)_2$ (**15**). The complex **15** was an internal standard since it was studied in other mixture (Fig. S5E).

## Schematic drawing of the studied complexes

**1:** 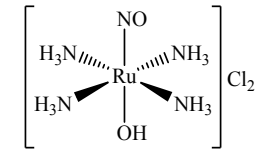

**2:** 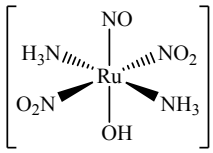

**3:** 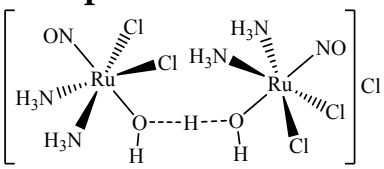

**4:** 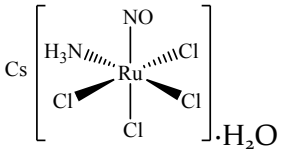

**5:** 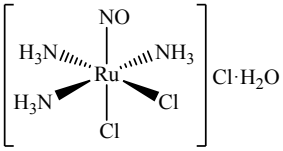

**6:** 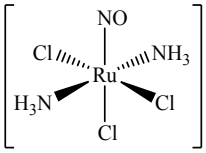

**7:** 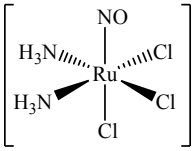

**8:** 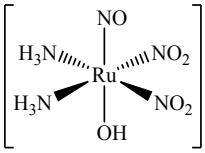

**9:** 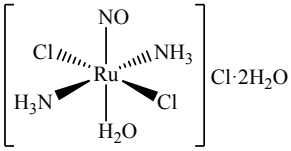

**10:** 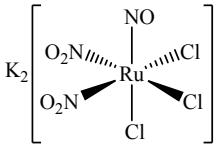

**11:** 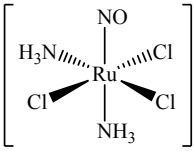

**12:** 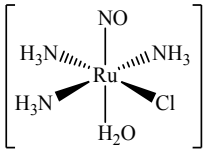

**13:** 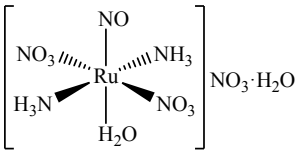

**14:** 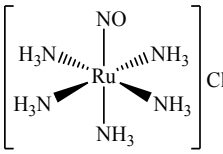

**15:** 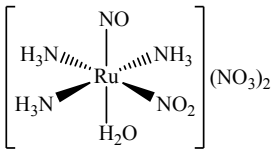

**16:** 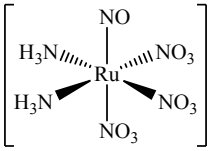

**17:** 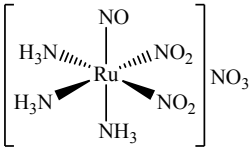

**18:** 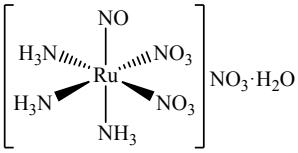

## References


(1) Il'yin, M. A.; Emel'anov, V. A.; Belyaev, A. V.; Makhinya, A. N.; Tkachev, S. V.; Alferova, N. I. New method for the synthesis of *trans*-hydroxotetraamminenitrosoruthenium(II) dichloride and its characterization. *Russ. J. Inorg. Chem.* **2008**, *53*(7), 1070.

(2) Schaniel, D.; Woike, T.; Boskovic, C.; Güdel, H. U. Evidence for two light-induced metastable states in $Cl_3[Ru(NH_3)_5NO]H_2O$. *Chem. Phys. Lett.* **2004**, *390*(4-6) 347.

(3) Il'in, M. A.; Kabin, E. V.; Emel'yanov, V. A.; Baidina, I. A.; Vorob'yov, V. A. *trans*-dinitro-and *trans*-dinitratoruthenium complexes $[RuNO(NH_3)_2(NO_2)_2(OH)]$ and $[RuNO(NH_3)_2(H_2O)(NO_3)_2]NO_3{\cdot}H_2O$. *J. Struct. Chem.* **2009**, 50(2), 328.

(4) Vorobyev, V.; Emelyanov, V. A.; Valuev, I. A.; Baidina, I. A. Nitrosyl cis-dichlorodiammine ruthenium complex with bridging $H_3O_2^-$ ligand. *Inorg. Chem. Commun.* **2017**, *76*, 40.

(5) Vorobyev, V.; Emelyanov, V. A.; Plusnina, O. A.; Makarov, E. M.; Baidina, I. A.; Smolentsev, A. I.; Tkachev, S. V.; Asanova, T. I. Triammine fac and mer Coordination for Ruthenium–Nitrosyl Complexes: Synthesis and Characterization of $[RuNO(NH_3)_3Cl_2]Cl$. *Eur. J. Inorg. Chem.* **2017**, (5), 971.

(6) Il'In, M. A.; Emel'yanov, V. A.; Baidina, I. A. Structure and synthesis of nitrosoruthenium trans-diammines $[Ru(NO)(NH_3)_2Cl_3]$ and $[Ru(NO)(NH_3)_2(H_2O)Cl_2]Cl{\cdot}H_2O$. *J. Struct. Chem.* **2008**, *49*(6), 1090.

(7) Sinitsyjn, N. M.; Svetlov, A. A.; Bryjkova, N. V. Synthesis and investigation into diammine complexes of nitrosylosmium and nitrosylruthenium. *Koord. Khim.* **1976**, *2*(5), 662.

(8) Vorobyev, V.; Kostin, G. A.; Kuratieva, N. V.; Emelyanov, V. A. Two Oxygen-Coordinated Metastable Ru–ON States for Ruthenium Mononitrosyl Complex. *Inorg. Chem.* **2016**, 55(18), 9158.

(9) Emel'yanov, V. A.; Baidina, I. A.; Gromilov, S. A.; Virovets, A. V.; Belyaev, A. V. Synthesis, Formation Mechanism, and Crystal Structure of the Nitrosoruthenium(II) Nitrochloride Complex *Fac*-$K_2[RuNO(NO_2)_2Cl_3]$. *J. Struct. Chem.* **2002**, *43*(2), 304.

(10) Emel'yanov, V. A.; Baidina, I. A.; Gromilov, S. A.; Vasiliev, A. D.; Belyaev, A. V. Synthesis and Crystal Structure of Nitrosoruthenium Triammino Complex $[RuNO(NH_3)_3Cl(H_2O)]Cl_2$. *J. Struct. Chem.* **2000**, *41*(6), 1030.

(11) Il'in, M. A.; Emel'yanov, V. A.; Baidina, I. A.; Alferova, N. I.; Korol'kov, I. V. Study of nitrosation of hexaammineruthenium(II): Crystal structure of *trans*-$[RuNO(NH_3)_4Cl]Cl_2$. *Russ. J. Inorg. Chem.* **2007**, *52*(1), 62.

(12) Schaniel, D.; Woike, T.; Boskovic, C.; Güdel, H. U. Evidence for two light-induced metastable states in $Cl_3[Ru(NH_3)_5NO]H_2O$. *Chem. Phys. Lett.* **2004**, *390*(4-6) 347.

(13) Vorobyev, V.; Kabin, E. V.; Emelyanov, V. A.; Baidina, I. A.; Korolkov, I. V. Synthesis and crystal structure of mer-nitroaquatriamminenitrosylruthenium(II) nitrate $[RuNO(NH_3)_3(NO_2)(H_2O)](NO_3)_2$. *Inorg. Chem. Commun.* **2016**, *68*, 1.

(14) Kabin, E. V.; Emel'yanov, V. A.; Vorob'yev, V. A.; Alferova, N. I.; Tkachev, S. V.; Baidina, I. A. Reaction of *trans*-$[RuNO(NH_3)_4(OH)]Cl_2$ with nitric acid and synthesis of ammine (nitrato)nitrosoruthenium complexes. *Russ. J. Inorg. Chem.* **2012**, 57(8), 1146.

(15) Vorobyev, V.; Baidina, I. A.; Korolkov, I. V.; Emelyanov, V. A. to be published

(16) Güida, J. A.; Piro, O. E.; Schaiquevich, P. S.; Aymonino, P. J. Infrared absorption spectra of electronically excited long-lived metastable states in $Na_2[Ru(CN)_5NO]\cdot 2H_2O$. *Solid State Commun.* **1997**, *101*(6), 471; Güida, J. A.; Piro, O. E.; Aymonino, P. J. Infrared absorption spectra of sodium pentacyanonitrosylosmate(II) dihydrate in two excited electronic metastable states. *Inorg. Chem.* **1995**, *34*(16), 4113.

(17) Sanz García, J.; Alary, F.; Boggio-Pasqua, M.; Dixon, I. M.; Malfant, I.; Heully, J. L. Establishing the two-photon linkage isomerization mechanism in the nitrosyl complex *trans*-$[RuCl(NO)(py)_4]^{2+}$ by DFT and TDDFT. *Inorg. Chem.* **2015**, *54*(17), 8310; Talotta, F.; Heully, J. L.; Alary, F.; Dixon, I. M.; González, L.; Boggio-Pasqua, M. Linkage photoisomerization mechanism in a photochromic ruthenium nitrosyl complex: new insights from an MS-CASPT2 study. *J. Chem. Theory Comput.* **2017**, *13*(12), 6120.

(18) Van der Maas, J. H.; Tolk, A. The influence of moisture on potassium bromide disks used in infrared spectrometry. *Spectrochim. Acta*, **1962**, *18*(2), 235.